JOURNAL OF THERMOPHYSICS AND HEAT TRANSFER
Vol. 24, No. 3, July–September 2010

Experimental Study of Graphite Ablation in Nitrogen Flow, Part II: Further Numerical Analysis

Toshiyuki Suzuki* and Kazuhisa Fujita†
Japan Aerospace Exploration Agency, Tokyo 182-0012, Japan
and
Takeharu Sakai‡
Nagoya University, Aichi 464-8603, Japan

DOI: 10.2514/1.43264

The ablative behavior of graphite heated in an inductively coupled plasma wind tunnel is analyzed using an integrated computational method to examine the probability value of nitridation reaction occurring at graphite surface. In this method, the plasma torch freestream condition at the entrance of the test chamber is evaluated by calculating the flows in the plasma torch. The thermal response of the graphite test piece is calculated by loosely coupling the thermochemical nonequilibrium fluid dynamics code and two-dimensional heat conduction equation solver using the freestream condition so valuated. Using a computational tool, surface contours of the graphite test piece at several time steps are calculated by varying the probability value of nitridation reaction and are compared with those measured in the heating test. The effect of impurities remaining in the test chamber is also taken into account. As a result of the study, it is suggested that a probability value of 0.003 for nitridation reaction is reasonable to explain the amount of mass loss of the graphite test piece in the heating test.

Nomenclature

c_p	=	specific heat at constant pressure, J/(kg · K)
J_s	=	mass flux of species, kg/(m^2 · s)
k	=	surface reaction velocity, m/s
M_s	=	molecular weight of species s, kg/mol
R	=	universal gas constant, 8.314 J/(mol · K)
r	=	mass-loss rate, kg/s
S	=	recession, m
s	=	mass-loss rate, m/s
T	=	temperature, K
α	=	reaction probability
ρ	=	density, kg/m^3

Subscripts

g	=	graphite
nit	=	nitridation reaction
oxi	=	oxidation reaction

I. Introduction

THIS study is the second part of a two-part work that follows [1], in which the rate of nitridation reaction on a graphite surface,

$$\mathrm{N} + \mathrm{C}(s) \rightarrow \mathrm{CN} + 0.35\ \mathrm{eV} \tag{1}$$

was investigated. A series of heating tests of graphite test pieces is conducted in high-temperature nitrogen flows produced in an inductively coupled plasma (ICP) heated wind tunnel. In the tests, the amount of mass loss of the graphite test piece was evaluated by comparing the weights of test piece between before and after heating. Numerical analysis of flowfield around the test piece was made to determine the number density of atomic nitrogen onto the graphite surface. Using the measured mass loss of test piece and the calculated number density of atomic nitrogen, the probability value of nitridation reaction was estimated by using a relation based on a kinetic theory. The obtained value was 0.003 for the surface temperature of about 1900 K. The probability value of the nitridation reaction on graphite was also deduced in a recent study made by Park and Bogdanoff [2] using an experimental approach different from our previous one. The probability value obtained by Park and Bogdanoff was much larger than the present one by a factor of 100. The exact cause of the reason for this discrepancy is unknown at present.

In our independent effort, an integrated computational method was developed to calculate the thermal response of the carbon phenolic ablator under an arcjet flow condition [3]. In this method, the ablative behavior of the material is calculated accounting for the interaction of the arcjet freestream with the ablated species through a loosely coupling method between the shock-layer computational fluid dynamics (CFD) code and a thermal response code named SCMA2. The calculated result showed that the qualitative characteristics of surface recession and shape change of ablative test piece could be changed if the thermal response of ablator was not analyzed with the coupled manner. Such a coupled approach was not included in the method used in [1] to calculate the atomic nitrogen value onto the ablating graphite surface. Assuming that such a detailed approach with a coupled manner is more accurate, the cause of the reason for the discrepancy between our probability value and that of Park and Bogdanoff [2] might have been due to the inadequacy in our previous computational approach. The reason for the study documented in this article is to investigate whether or not the thermal response analysis was the cause for the discrepancy.

The present study aims to examine the accuracy of the probability value of nitridation reaction obtained in our previous study. For this purpose, we first establish an integrated computational methodology that can analyze the nitridation of the graphite under the ICP wind-tunnel condition. The developed method is an upgrade version of our previous method. In the present approach,

1) The thermal response of the graphite test piece is calculated using two-dimensional heat conduction equation by accounting for the interacting behavior between high-temperature ICP wind-tunnel flows and the ablated species from graphite.

Presented as Paper 1217 at the 46th AIAA Aerospace Sciences Meeting and Exhibit, Reno, NV, 7–10 January 2008; received 16 January 2009; revision received 18 February 2010; accepted for publication 25 February 2010.

*Researcher, Institute of Aerospace Technology, 7-44-1 Jindaiji Higashi-machi, Chofu-shi; suzuki.toshiyuki@jaxa.jp. Member AIAA.
†Senior Researcher, Institute of Aerospace Technology, 7-44-1 Jindaiji Higashi-machi, Chofu-shi; Member AIAA.
‡Associate Professor, Department of Aerospace Engineering, Furo-cho, Chikusa-ku, Nagoya; Senior Member AIAA.

2) The flowfield around the graphite test piece is calculated using a thermochemical nonequilibrium CFD code with nitridation reaction by accounting for the ICP wind-tunnel freestream condition.

3) The freestream condition at the entrance of test chamber is estimated by calculating the flowfield in the plasma torch numerically.

The developed method is then applied to numerically simulate the heating environments over the graphite test piece for ICP wind-tunnel operating conditions. The surface shape of the graphite test piece is calculated by accounting for possible surface reaction processes. Of these processes, several surface reaction probability values for nitridation reaction are tested to compare the surface shape of the graphite test piece between calculation and measurement to examine the accuracy of the probability value obtained in our previous study. In addition, the surface oxidation process is incorporated to examine a possible impact on the mass loss due to the impurities included in the ICP freestream flows. Based on the spectroscopic measurement made by Fujita et al. [4], a small amount of impurities (e.g., O and H_2O) was observed in the high-temperature nitrogen flows even if the test chamber was evacuated before the wind-tunnel operation. Thus, the measured mass loss of graphite in the ICP wind-tunnel operation might be attributed not only to the nitridation but also to the oxidation by atomic oxygen, leading to an erroneous probability value for nitridation reaction. The possible error in the measured mass loss will be evaluated by using the developed method for the case that a small amount of oxygen is included in the ICP freestream.

II. Experimental Configurations

The heating tests were conducted in the 110 kW ICP wind-tunnel facility in Japan Aerospace Exploration Agency (JAXA). Though the details of the experiment can be found in [1], the experimental configurations are described briefly here. The facility consists mainly of a plasma torch and a test chamber. The plasma torch is made of a quartz cylindrical tube with an induction coil of three-turn. The quarts tube has a diameter of 75 mm and a length of 250 mm. The wind tunnel is usually operated at a frequency of 1.78 MHz by water-cooling the quartz tube.

A graphite test piece was exposed to the hot nitrogen flow. The test piece has a flat-shaped nose with a diameter of 3 mm and a length of 25 mm. The ICP wind tunnel is operated under electrical power input from 70 to 110 kW with constant mass flow rate of 2 g/s, realizing a mass-averaged enthalpy ranging from 15 to 20 MJ/kg. The forefront of the test piece was placed at 566 mm from the quartz tube exit. The surface temperature of the test piece exposed to the hot nitrogen flow was measured by a one-color optical pyrometer. After testing, the test pieces were weighed to obtain the amount of mass loss. From the experimental results, the reaction probability was deduced for each of the test pieces. The deduced value was ranging from 0.0025 to 0.0032, and an averaged value was 0.0028.

To remove the impurities such as molecular oxygen remained in the wind tunnel, the test chamber is purged: the chamber is filled with nitrogen gas at once, and the chamber was evacuated after that. This procedure was repeated 3 times before each of the wind-tunnel operations. Accordingly, in our previous study, the amount of atomic oxygen remaining in the test section was assumed to be negligibly small. However, based on the radiation emission spectroscopic data [4] taken in the test chamber with the same replacement technique, the mole fraction of the atomic oxygen remaining in the test section was found to be a maximum of 0.1%. Because whether such an amount of atomic oxygen could affect the amount of mass loss of graphite is unknown, a coupled calculation will be made additionally by accounting for the presence of atomic oxygen in the test chamber.

III. Numerical Methods

A. Outline of Simulation and Computational Meshes

In the course of the simulation, the temporal shape change of the graphite test piece is obtained by calculating the thermal response of graphite through a coupled manner developed in our previous study [3]. In the coupled method, the thermal response is analyzed by using different computational tools. The flowfield calculations are made separately for the plasma torch and for the test chamber. Although some of the details are given in our previous study, the brief explanation of the procedure is explained below for completeness.

1. *Thermal Response Analysis of Graphite Test Piece*

The thermal response of the graphite test piece is calculated by solving two-dimensional heat conduction equation numerically. The equation is discretized by using the finite volume method. Solutions are obtained by integrating the discretized equation implicitly in time. Thermal properties used in the present calculation are as follows: The graphite test piece used in the heating tests was isotropic one (Fine Carbon G530[§]) manufactured by Tokai Carbon Company, Ltd. According to the material sheet published by the manufacturer, the density and the thermal conductivity for the present graphite material are 1820 $\mathrm{kg/m^3}$ and 104.0 $\mathrm{W/(m \cdot K)}$, respectively. Because the temperature dependence of the thermal conductivity used is presently unknown, the conductivity value is assumed to be constant in the present study. The specific heat of graphite is taken from [5], and is expressed as

$$c_p = \frac{c_\infty T}{\sqrt{T^2 + (c_\infty / c_1)^2}} \tag{2}$$

where $c_\infty = 2300$ J/(kg · K), and $c_\infty / c_1 = 800$ K.

The thermal response analysis needs two boundary conditions: heat flux and mass-loss rate. The heat fluxes and mass-loss rate at each position along the graphite surface must be known as a function of time. An iterative procedure is used to obtain the consistency of the two boundary conditions between the heat conduction analysis and the flowfield calculation over the test piece, which will be explained in the next subsection. Based on our experience in our previous work [3], three iterations are needed to obtain convergence at a given time. This procedure must be repeated to obtain a time-dependent solution for total testing time.

Because this procedure is very time-consuming, several time points need to be chosen practically. Ideally, the interval between two time points should be short because the phenomenon over the graphite test piece is unsteady. When we made a coupling calculation by setting a time interval equally to be 100 seconds until the end of testing, the calculated surface contour of the test piece was totally different from the heated test piece. This qualitatively different contour was likely due to insufficient time resolution during the first 100 seconds from the beginning of testing: In that case, the temperature and atomic nitrogen density distributions over the surface of the test piece changed dramatically in the first 50 seconds, but remained keeping unphysical after $t = 100$ s. As a result, we added three time points prior to $t = 100$ s and 12 points at $t_i = 10$, 30, 50, 100, 200, 300, 400, 500, 600, 700, 800 and 900 s ($i = 1, 2, \cdots, 12$) were selected for the present study. The computing time of the coupled calculation is about 240 h (10 days) by using two dual core processors (Intel® Xeon® 5050) installed in a Dell Precision workstation 690.

2. *Flowfield Analysis*

The freestream condition at the entrance of the test chamber is obtained by numerically simulating the flowfield in the plasma torch with a thermochemical equilibrium Navier-Stokes code. For the calculation within the plasma torch, Maxwell's equations are solved and its electromagnetic effect is coupled in a loosely manner to calculate the Joule heating through the induction current. Other details are given in the previous work [6]. At the center of the plasma torch exit, the calculated temperature varies from 7000 to 9800 K, depending on the input power ranging from 70 to 110 kW, while the

[§]Data available online at http://www.tokaicarbon.co.jp/en/products/fine_carbon/isotropic.html [retrieved 1 June 2007].

horizontal component of velocity vector varies from 160 to 250 m/s, and the degree of dissociation varies from 0.78 to 0.96, respectively. The flow property at the plasma torch exit varies in a radial direction by about 8% until about $r = 0.01$ mm as compared with its centerline value. The obtained flow density, temperature, two velocity components and mass fraction of chemical species along the plasma torch exit are used in the flowfield analysis in the test chamber as an inflow boundary condition, which will be explained next.

The flowfield over the graphite test piece in the test chamber is assumed to be axisymmetric and viscous in thermochemical nonequilibrium state. To calculate the nonequilibrium thermochemistry in the flowfield, Park's two-temperature model is used with 17 chemical species (N, O, N_2, O_2, NO, N^+, O^+, N_2^+, O_2^+, NO^+, C, C_2, CN, CO, C_3, C^+, and e−). The nitridation and oxidation reaction at the graphite surface is modeled in the calculation. The nitridation and oxidation models will be explained later. The freestream condition calculated by the plasma torch analysis is applied at the entrance of the test chamber. The flow properties at the boundary between the graphite test piece and the nonequilibrium flowfield are calculated using a coupled manner mentioned earlier. Adiabatic and no-slip wall conditions are imposed at the test-chamber wall surface and at the surface of the firebrick attachment holding the graphite test piece, respectively.

The present analysis method to predict the freestream conditions of the ICP wind tunnel was validated against experimental data obtained by Fujita et al. [4]. In their work [4], the emission spectra from the flows in the test chamber of the ICP wind tunnel were measured. The measurements were made at 372 mm from the coil center (at 5 mm away from the graphite test piece surface). By comparing the measured spectra with that calculated by using the computer code SPRADIAN2, molecular temperature and species concentrations were determined for the nitrogen test flow at same wind-tunnel conditions used in this study. In [1], calculated freestream temperature, density, and mass fraction of atomic nitrogen were compared with those measured. It was shown that the agreement between the measurement and the present calculation is fairly good.

3. Mesh

The computational mesh system used in this study is shown in Figs. 1a and 1b. The plasma torch analysis is conducted by using two different computational meshes: one for the flowfield calculation denoted by zone 1, and the other for the electromagnetic field given in zone 2, as shown in Fig. 1a. The number of grid points for zone 1 and zone 2 is 90×44, and 128×63, respectively. The number of 69×69 grid points is used in zone 3 for the flowfield computation around the graphite test piece. The computational meshes used in the thermal response calculation are shown in Fig. 1b. Note that the computational domain for the graphite is divided into two zones: zone 4 has 47×25 and zone 5 has 20×28 grid points. Zone 4 and zone 5 are required to account for the surface shape change of graphite. When the shape of the graphite test piece changes, the outer boundary in zone 4 (corresponds to the surface of the graphite test piece) is redefined accordingly and new numerical mesh system is redrawn to construct zones 3 and 4. The grid points in zone 5 remain fixed in the course of simulation.

The solution was obtained on a finer computational mesh system by using four times the number of mesh points in zones 3, 4, and 5, as compared with the standard mesh given in Fig. 1b. The calculated surface shape of the graphite test piece is compared between the finer and the standard mesh systems. The result shows that no significant difference is seen between the two mesh systems. In addition, the effect of the minimum mesh interval in normal to the surface of the graphite test piece on the heat flux distribution at the surface is examined. The obtained result indicates that there was little difference when the mesh interval is reduced from 1×10^{-6} to 1×10^{-7} m. Note that the minimum mesh size adjacent to the surface is 1×10^{-6} m in the standard mesh. Based on this grid refinement study, we will present calculated results hereafter by using the standard mesh.

B. Nitridation and Oxidation Model

In the present study, we consider the nitridation reaction and the possible oxidation reaction that occur at the graphite surface. The

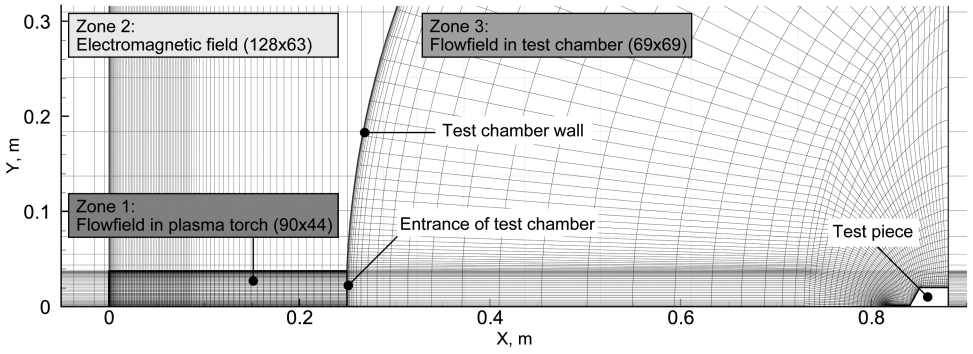

a) Overall view of computational mesh system

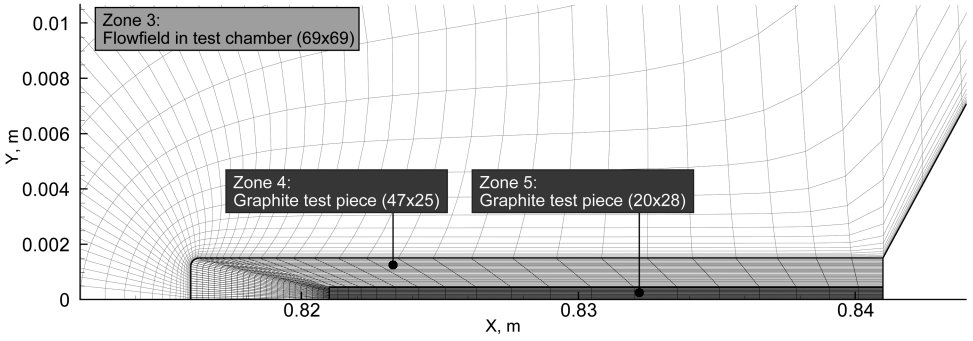

b) Close-up view around graphite test piece

Fig. 1 Computational meshes for thermal response analysis of the graphite test piece under an ICP wind-tunnel condition.

mass flux of CN due to nitridation, and that of CO due to oxidation are given by as follows:

$$J_{\mathrm{CN}} = \frac{M_{\mathrm{CN}}}{M_{\mathrm{N}}}\rho_{\mathrm{N}}k \tag{3}$$

$$J_{\mathrm{CO}} = \frac{M_{\mathrm{CO}}}{M_{\mathrm{O}}}\rho_{\mathrm{O}}k \tag{4}$$

The symbol k denotes surface reaction velocity, and is given by

$$k = \frac{\alpha}{4}\sqrt{\frac{8RT}{\pi M_s}} \tag{5}$$

where α and T denote the reaction probability and the surface temperature, respectively. Two different probability values are tested for the nitridation reaction: $\alpha_{\mathrm{nit}} = 0.003$ deduced in our previous study [1], and $\alpha_{\mathrm{nit}} = 0.3$ given by Park and Bogdanoff [2]. As will be shown later, the calculated surface shape of the graphite test piece differs much between these two α_{nit} values.

The reaction probability for the oxidation reaction is taken from [7], and is expressed as

$$\alpha_{\mathrm{oxi}} = 0.63\exp(-1160/T) \tag{6}$$

The graphite surface is assumed to be noncatalytic to atomic nitrogen or atomic oxygen for all the computed cases in the present study, because it is found in a past experimental study that the catalytic recombination reaction by those atomic species hardly occurs at graphite surface [8–10].

It should be noted that the flowfield over the ablating graphite is calculated by accounting for the modified shape of the graphite via the coupled calculation. The mass-loss rate at each grid point is obtained from the CFD solutions as

$$s = \frac{M_{\mathrm{C}}}{M_{\mathrm{CN}}}\frac{J_{\mathrm{CN}}}{\rho_g} + \frac{M_{\mathrm{C}}}{M_{\mathrm{CO}}}\frac{J_{\mathrm{CO}}}{\rho_g} \tag{7}$$

The amount of surface recession at a certain time point is obtained by integrating the mass-loss rate with time and is given by as follows:

$$S = \int_0^{t_i} s\,\mathrm{d}t \tag{8}$$

In the course of the present analysis, the mass fluxes of CN and CO are obtained from the converged solution of the flowfield analysis around the graphite in the test chamber. With the mass flux values so obtained, the amount of surface recession in the normal direction to the surface is calculated by using Eqs. (7) and (8).

IV. Results and Discussions

A coupled thermal response inside a graphite test piece is calculated using the reaction probability value of 0.003 for three ICP wind-tunnel conditions: 70, 90, and 110 kW. The thermal response calculation continues up to $t = 900$ s for the case of 70 kW and to $t = 600$ s for the cases of 90 and 110 kW. The initial conditions for the chemical composition of the ambient gas in the test chamber are shown in Table 1. Unless otherwise noted, the calculated results presented here are obtained by assuming that the amount of atomic oxygen remaining in the test chamber is zero (case 1). The results calculated by accounting for impurities remaining in the test chamber (case 2 or 3) will be shown later.

A. Outline of Thermal Response of Graphite Test Piece Under ICP Wind-Tunnel Condition

Calculated temperature contours are shown in Figs. 2a–2d for the case of 70 kW. Figure 2a–2d correspond to the time period at $t = 0$, 300, 600, and 900 s, respectively. One can see from these figures that the temperature within the graphite increases from the onset of heating. The temperature inside the graphite test piece is nearly constant at each time. This trend is due to the fact that the thermal conductivity of the graphite used in the heating tests is relatively high (104.0 W/m-K), and that the thermal conduction is sufficiently fast for the length of the graphite used. A similar trend is obtained for the cases of 90 and 110 kW, though the results are not shown here.

One can also see from Figs. 2a–2d that the surface of the graphite test piece is receding due to the nitridation reaction occurring at the surface. By comparing the calculated results between Figs. 2a and 2d, the difference of the surface shape between before and after heating is clearly recognized. As time elapses, the frontal surface of the rod becomes sharper.

B. Temporal Variations of Surface Temperature and Atomic Nitrogen Density Around Graphite

In [1], the reaction probability was deduced based on the assumption that the surface temperature and the atomic nitrogen density values were constant during the testing. Though the experimental data showed that this assumption was likely to be valid, especially for the surface temperature, further numerical study would be warranted to check the validity of the assumption. For this purpose, the effect of the time-dependency of the surface temperature and the atomic nitrogen density on the computed solutions is examined in more detail. Calculated results presented here are also obtained by using $\alpha_{\mathrm{nit}} = 0.003$.

In Fig. 3, the calculated time history of surface temperature at the stagnation point is plotted against time for the case of 70 kW. A similar trend is seen for the cases of 90 and 110 kW, and the results are omitted here. For the purpose of comparison, the measured values of surface temperature are also shown in Fig. 3. In the measurement, the surface temperature of the test piece was measured by a one-color optical pyrometer. The experimental error was estimated to be less than 5%. As shown in the figure, the surface temperature increases rapidly from the onset of heating. After that, the surface temperature continues to increase slightly. This small temperature rise is because the nose tip of the graphite test piece becomes sharp due to heating. As a result, the heat flux at the stagnation point increases slightly with time. Nevertheless, the calculated temperature rise rate during 600 s of exposure time is only about 0.25 K/s: the assumption of constant surface temperature is believed to be valid. As shown, the calculation predicts the measure temperature history fairly well.

Figure 4 shows the surface temperature distributions along the surface of the graphite test piece at several time points. The results are presented for the case of 70 kW. One can see from the figure that the temperature along the graphite surface increases over the entire region from the stagnation point to the side surface. The surface temperature decreases only slightly away from the stagnation point: the temperature difference between at the stagnation point and at the end point on the side surface is about 100 K at most.

Figure 5 shows the temporal variations of atomic nitrogen density at the stagnation point. The results are presented for the cases 70, 90, 110 kW. From the figure, the density value of atomic nitrogen increases with the working power. The reason for this difference is that the degree of dissociation of nitrogen increases with the increase in working power. One can see that the atomic nitrogen density is

Table 1 Calculation conditions in the test chamber.

	Ambient pressure, kPa	Chemical composition, N_2:O_2 by mole	Notes
Case 1	10	100:0	Represents ideal flowfield with no impurities
Case 2	10	99:1	Represents flowfield in test chamber after replacement of ambient gas
Case 3	10	79:21	Represents flowfield in test chamber without replacement of ambient gas

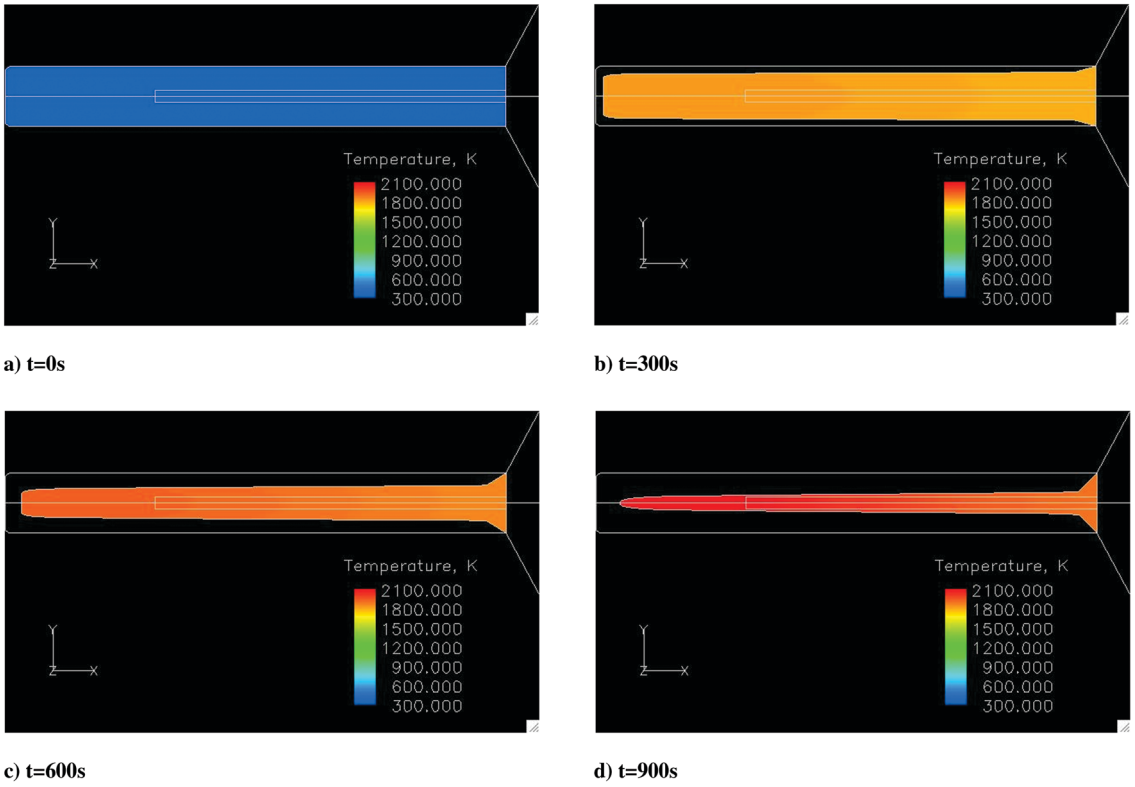

Fig. 2 Calculated temperature contours of the graphite test piece under the ICP wind-tunnel test condition: a) $t = 0$ s from onset of heating, b) $t = 300$ s from onset of heating, c) $t = 600$ s from onset of heating, and d) $t = 900$ s from onset of heating.

almost constant during 600 s, except for the beginning of exposure. This trend is because the temperature rise rate is so small, except for the beginning of exposure that the surface temperature continues to be almost constant during the heating as shown in Fig. 3. From this result, we judge that the assumption of constant atomic nitrogen density made in our previous study is likely to be valid.

Figure 6 shows the distributions of atomic nitrogen density along the graphite surface at several time points for the case of 70 kW. The results are presented for the cases with and without thermal response coupling. The calculated result for the uncoupled case will be explained later. As shown in the figure, the number density of atomic nitrogen at the stagnation point is slightly larger than that at the side surface at $t = 10$ s. After that time, however, the atomic nitrogen density reduces gradually, and the variation of the atomic nitrogen density over the entire surface becomes small. This trend is consistent with that seen in the surface temperature distribution along the graphite surface, as was seen in Fig. 4.

From Fig. 6, the atomic nitrogen density at the stagnation point for the case without thermal response coupling is four times higher than that for the case with thermal response coupling. This result implies that the number density of atomic nitrogen might be overestimated in our previous study [1] by a factor of 4. If the smaller density value obtained by the present coupled approach would be true, the probability value of the nitridation reaction could be reduced to be $0.003/4 = 0.00075$ because the nitridation probability value was obtained in our previous work through the following relation:

$$r = \frac{M_C}{M_N} A \rho_N k \tag{9}$$

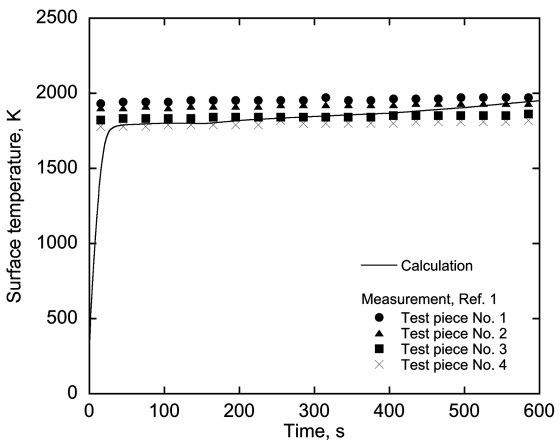

Fig. 3 Comparison of surface temperature variations between calculation and measurement for the case of 70 kW.

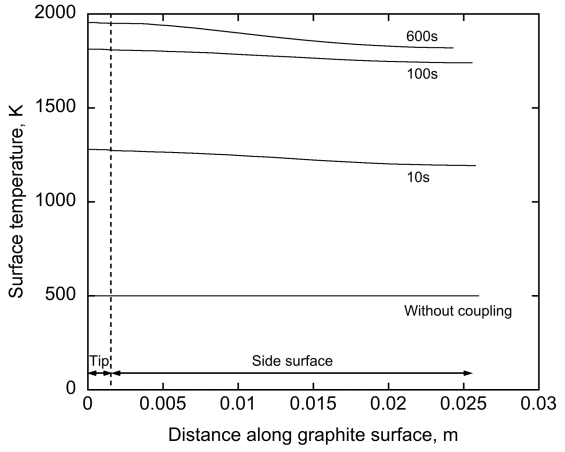

Fig. 4 Temporal changes of surface temperature distribution for the case of 70 kW.

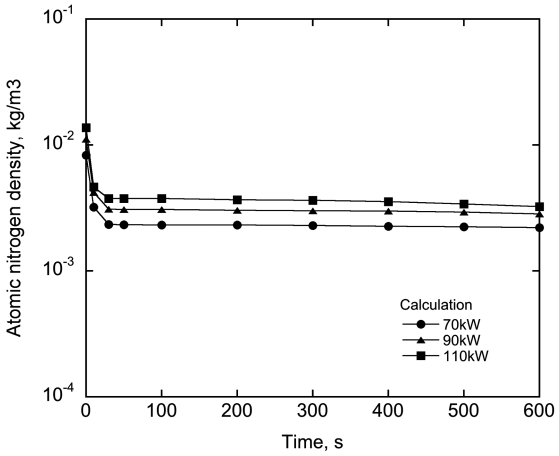

Fig. 5 Temporal variations of atomic nitrogen density at the stagnation point.

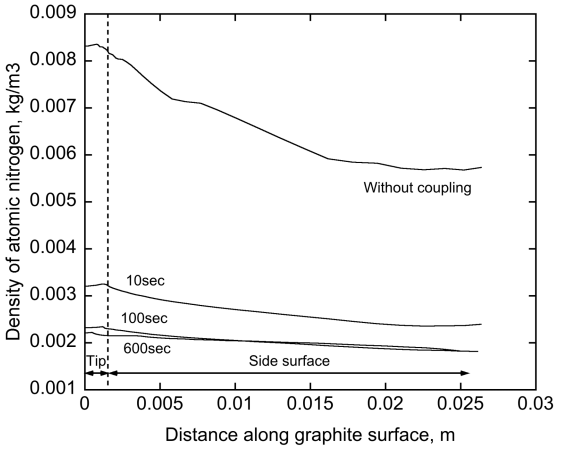

Fig. 6 Temporal changes of atomic nitrogen density distribution for the case of 70 kW.

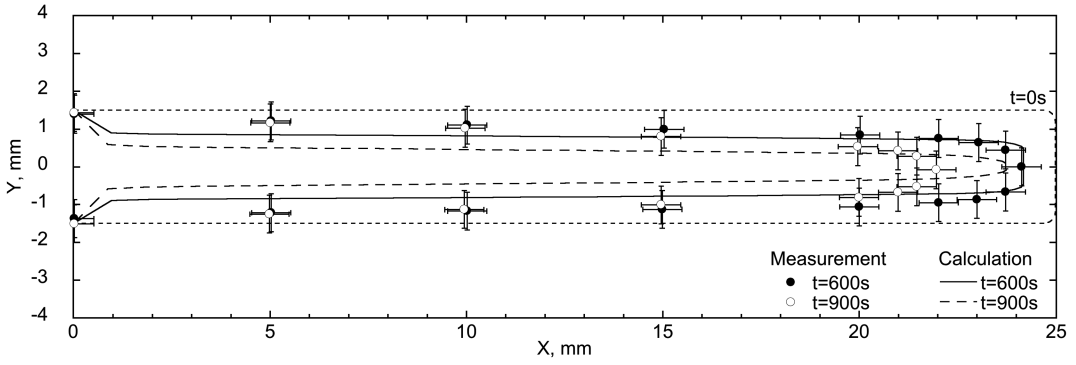

a) 70kW

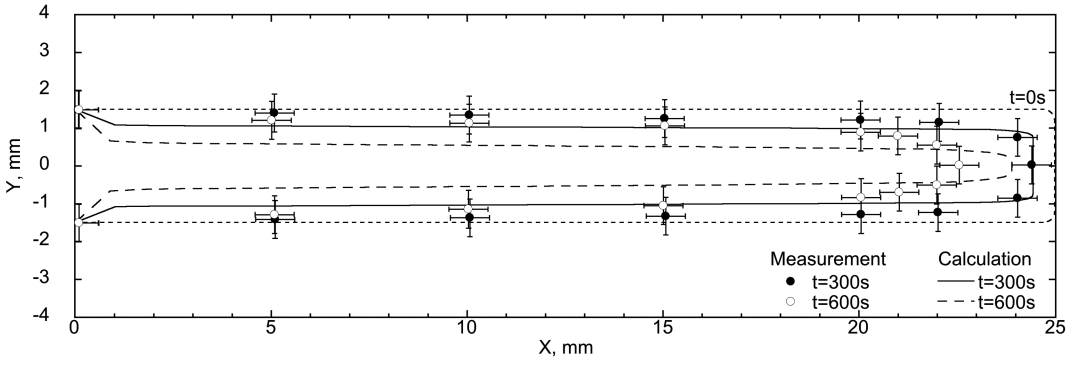

b) 90kW

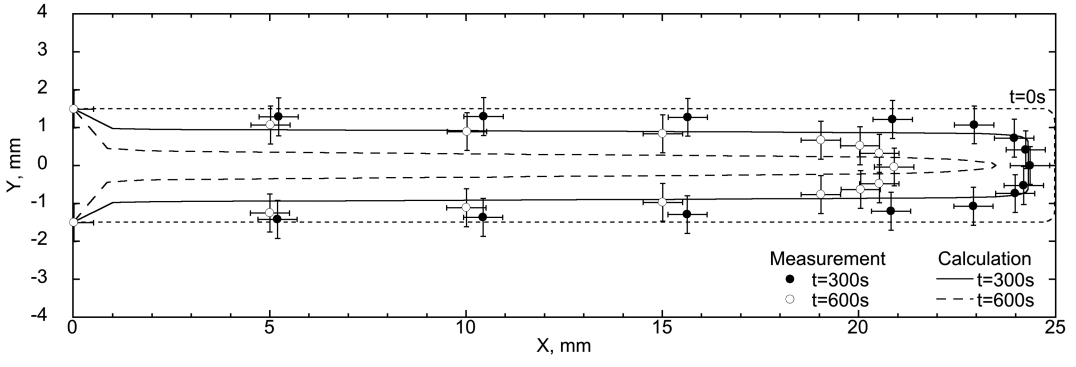

c) 110kW

Fig. 7 Comparison of surface shape of the graphite test piece between calculation and measurement.

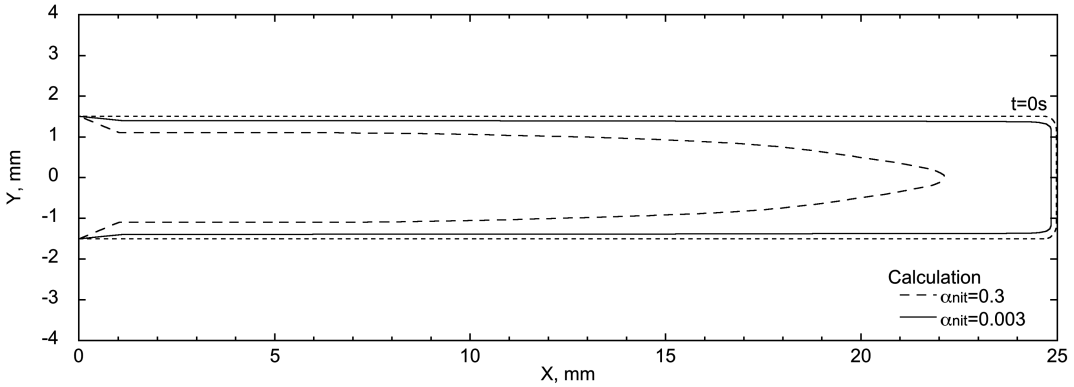

Fig. 8 Comparison of surface shape of the graphite test piece between two different probability values.

The value of surface area of the graphite test piece, A in the above equation, was taken to be a constant value. However, because the shape of the graphite test piece was changing during the heating due to nitridation reaction, the assumption of the constant surface area would be unrealistic: a possible value of the surface area of the graphite test piece could be reduced one-third from the shape of the heated test piece. With this revised value of surface area, the probability value of nitridation could be increased up to $0.003 \times 3 = 0.009$. When both of revised atomic nitrogen density and surface area values are accounted for, the nitridation probability would be $0.003 \times 3/4 = 0.0025$, which is nearly the same of the probability value of 0.003 used in the present study. Note that the range of the estimated nitridation probability value is much lower than the value of 0.3 predicted by Park and Bogdanoff [2].

C. Comparison of Surface Contour of Graphite Between Calculation and Experiment

Figures 7a–7c shows the comparison of surface contours of the graphite test piece after heating between calculation and experiment. Calculated results are obtained by a present coupled approach with $\alpha_{\text{nit}} = 0.003$. Experimental results are obtained as follows. After the heating tests, graphite test pieces were put on graph paper with a scale, and we took a photograph of each of them. The original coordinate data of the graphite surface were digitized by scanning the photograph. The experimental uncertainty of the coordinate data so digitized is estimated to be less than ± 0.5 mm.

In Fig. 7a, calculated surface contours at $t = 600$ and 900 s from the onset of heating are presented for the case of 70 kW. The recessed thickness of the heated test piece is given in the same figure. From the comparison between the calculation and the experiment, one can see that the calculated recessed thickness at $t = 600$ s is well within the error bars of the measured one. At $t = 900$ s, the calculation underestimates the measured value by about 2 mm at the stagnation point, and overestimates in the region of the side wall by 0.5 mm.

Comparisons of the surface contours for the cases of 90 and 110 kW are shown in Figs. 7b and 7c, respectively. In these figures, calculated surface contours at $t = 300$ s and 600 s are compared with those measured. For these cases, the general trend is similar to that observed for the case of 70 kW: the calculated recessed distance is smaller than the experimental one at the stagnation point; in contrast, the calculation overestimates the measured recession near the side wall.

The overestimation of the recessed thickness along the side surface in calculation is believed to be due to the fact that the temperature dependence is ignored in the reaction probability value used. With the constant probability value, the nitridation reaction is believed to proceed at almost the same rate along the surface under the present heating environment. This trend can be confirmed from the result that the computed recessed thickness at a point along the side surface is almost the same with that at the stagnation point. However, as shown in Figs. 4 and 6, the surface temperature and the density of atomic nitrogen are reduced continuously along the surface. Therefore, the nitridation reaction probability could be reduced, being affected by the flow condition upstream of a point along the surface. In addition, from the recent effort given by the authors [11], it was found that the probability value of nitridation could vary from 1.4×10^{-3} to 3.2×10^{-3} at the surface temperature ranging from 1400 to 2200 K. Such an effect of the temperature dependence of the nitridation reaction on the recession thickness of the stagnation-point region is beyond the scope of the present work and such a task will be left to the future.

To examine the impact due to the difference of probability values on the amount of mass loss of graphite, the solution is obtained by using the present coupled approach with the probability value of $\alpha_{\text{nit}} = 0.3$ for the case of 70 kW. The present calculation shows that the surface temperature for the case of $\alpha_{\text{nit}} = 0.3$ becomes about 200 K larger than that for the case of $\alpha_{\text{nit}} = 0.003$ at $t = 50$ s, and that the surface temperature continues to increase, and reaches about 2200 K at $t = 100$ s. The higher surface temperature for $\alpha_{\text{nit}} = 0.3$ is believed to mainly due to the higher heat flux by a smaller surface area as compared with the case of $\alpha_{\text{nit}} = 0.003$: the surface contour of the graphite test piece for the case of $\alpha_{\text{nit}} = 0.3$ tapers to a sharp point, unlike the surface contour for the case of $\alpha_{\text{nit}} = 0.003$, as shown in Fig. 8. Figure 8 shows the calculated surface contours at $t = 100$ s from the onset of heating for the probability value of $\alpha_{\text{nit}} = 0.3$. For the purpose of comparison, calculated result obtained by using $\alpha_{\text{nit}} = 0.003$ is also shown in the same figure. One can see that the surface contour of the graphite test piece for the case of $\alpha_{\text{nit}} = 0.3$ becomes shorter than that for the case of $\alpha_{\text{nit}} = 0.003$, and about one-third of graphite material is lost during the first 100 s. This trend is due to the fact that the mass-loss rate given in Eq. (7) becomes larger as the reaction probability increases. As a result, the amount of surface recession for the case of $\alpha_{\text{nit}} = 0.3$ becomes larger than that for the case of $\alpha_{\text{nit}} = 0.003$, as can be seen Eq. (8). Though the result is not shown here, the present calculation showed that if the coupled analysis continues up to $t = 600$ s using the reaction probability value of 0.3, almost all of the graphite test piece would be lost. Such a result contradicts the obtained result in the present experimental.

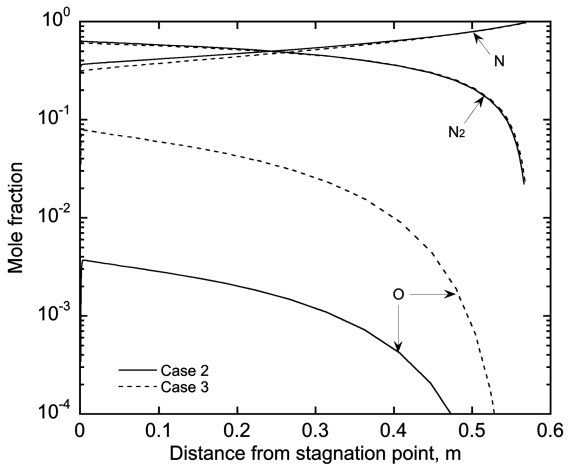

Fig. 9 Amount of atomic oxygen remaining in the test chamber.

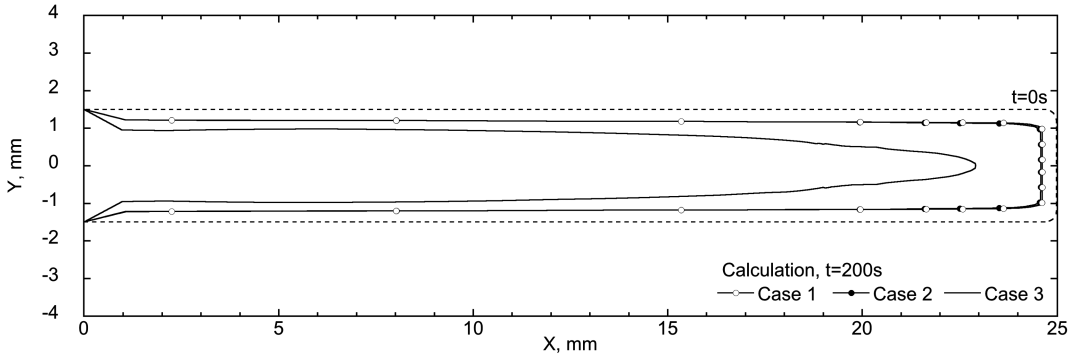

Fig. 10 Surface shape change due to oxidation by atomic oxygen remaining in the test chamber.

The sensitivity of the thermal conductivity value was examined for the case of 70 kW by varying the thermal conductivity value within 10% of the original value. It was found from the study that the surface temperature of graphite was slightly affected by the thermal conductivity value, while there was little difference in the amount of mass loss of the graphite test piece for those thermal conductivity values. This result is because the amount of mass loss of graphite is a function of the square root of the surface temperature, as given in Eqs. (3) and (5).

To study the effect of the following exchange reaction,

$$C + N_2 \leftrightarrow CN + N \tag{10}$$

the coupled analysis of flowfield and thermal response of graphite was additionally performed by ignoring this reaction for the case of 70 kW. The obtained surface contour of the graphite test piece at $t = 100$ s was compared with that calculated by taking account of the exchange reaction. Though the result is not shown here, the present calculation showed that if the exchange reaction of Eq. (10) was ignored, the amount of mass loss of graphite becomes small along the graphite surface by a factor of 2. In addition, the number density of atomic nitrogen decreased around the graphite surface when the exchange reaction was ignored, while that of molecular nitrogen increased. These phenomena are believed to occur because the production of atomic nitrogen decreases due to ignoring the exchange reaction. As a result, the number density of atomic nitrogen striking onto the graphite surface decreases along the wall surface.

D. Effect of Atomic Oxygen Remaining in Test Chamber

The effect of the impurities in the test chamber on calculated recession is examined by including molecular oxygen into the freestream flow. Two cases are considered for this purpose: In case 2, 1% molecular oxygen is included by mole. The amount of molecular oxygen so included is determined to give the same level of the atomic oxygen near the graphite rod as the one measured by Fujita et al. [4]; In case 3, 21% molecular oxygen is given by mole. This case represents a hypothetical one in which no replacement of the ambient gas inside the test chamber is made. For this case, the recession should be mainly due to oxidation reaction. The rate of oxidation is calculated by using Eq. (6), and the results for cases 2 and 3 will be compared with case 1, in which no impurities are contained in the flow.

The typical example of the converged solution for the flowfield calculation is shown in Fig. 9. In the figure, the mole fraction of atomic oxygen along the stagnation streamline for the case of 90 kW is shown for cases 2 and 3. One can see from the figure that the amount of atomic oxygen in the test chamber for case 2 becomes smaller than that for case 3, as expected. The test gas around the test piece contains almost 10% of atomic oxygen for the case 3, while its concentration becomes less than 0.1% for case 2. Note that the amount of atomic oxygen at the stagnation point for case 2 is as much as that of measured in the spectroscopic study made by Fujita et al. [4].

Figure 10 shows the calculated surface contours of the graphite test piece at $t = 200$ s for three test-chamber conditions. The results are obtained by a present coupled approach for the wind-tunnel condition of 90 kW. As shown in Fig. 10, the calculated surface contour for the case 2 duplicates well the solution for case 1. This result indicates that the effect of atomic oxygen remaining in the test chamber could become negligible if the concentration of atomic oxygen could be reduced to less than 0.1%. Based on this result, it is considered that almost all of mass loss of graphite obtained in our previous study attributed to nitridation reaction.

From the figure, it can be clearly recognized that the amount of mass loss of the graphite test piece for case 3 becomes larger than those for other cases. This trend is because the amount of atomic oxygen remaining in the test chamber is so large that the mass loss of the graphite test piece is occurring mainly by the oxidation reaction. This result implies that if the ambient gas in the test chamber was not replaced by using the nitrogen gas before the wind-tunnel operation, one could easily fail to estimate the rate of nitridation reaction from the experimental data.

V. Conclusions

Using the upgraded computational method, it is confirmed that an effective probability value for the nitridation reaction on ablating graphite surface is 0.003. The effect of atomic oxygen, which would be included in the inductively coupled plasma nitrogen flows as impurities, on the measured mass loss is found to be negligibly small. The reason for the difference of the probability value between the present study and Park and Bogdanoff's [2] study is still an unresolved issue. The impact of the nitridation reaction on ablative characteristics in flight environments should be examined to examine the differences between the two values.

Acknowledgment

This work was partly supported by the Grant-in-Aid for Young Scientists B (no. 20760553) from the Ministry of Education, Culture, Sports, Science, and Technology in Japan.

References

[1] Suzuki, T., Fujita, K., Ando, K., and Sakai, T., "Experimental Study of Graphite Ablation in Nitrogen Flow," *Journal of Thermophysics and Heat Transfer*, Vol. 22, No. 3, 2008, pp. 382–389. doi:10.2514/1.35082

[2] Park, C., and Bogdanoff, D. W., "Shock-Tube Measurement of Nitridation Coefficient of Solid Carbon," *Journal of Thermophysics and Heat Transfer*, Vol. 20, No. 3, 2006, pp. 487–492. doi:10.2514/1.15743

[3] Suzuki, T., Sakai, T., and Yamada, T., "Calculation of Thermal Response of Ablator Under Arcjet Flow Condition," *Journal of Thermophysics and Heat Transfer*, Vol. 21, No. 2, 2007, pp. 257–266. doi:10.2514/1.25499

[4] Fujita, K., Suzuki, T., Mizuno, M., and Fujii, K., "Comprehensive Flow Characterization in a 110-kW Inductively-Coupled-Plasma Heater," *Journal of Thermophysics and Heat Transfer*, Vol. 23, No. 4, 2009, pp. 840–843; also AIAA Paper 2008-1254, Jan. 2008.

doi:10.2514/1.43275
[5] Potts, R. L., "Application of Integral Methods to Ablation Charring Erosion, A Review," *Journal of Spacecraft and Rockets*, Vol. 32, No. 2, 1995, pp. 200–209.
doi:10.2514/3.26597
[6] Ando, K., Sakai, T., and Yamada, T., "Calculation of Flows in an Inductively Coupled CO_2 Plasma Wind Tunnel," *Symposium on Flight Mechanics and Astrodynamics*, Inst. of Space and Astronautical Sciences, Japan Aerospace Exploration Agency, Kanagawa, Japan, 2006, pp. 17–19 (in Japanese).
[7] Park, C., "Effect of Atomic Oxygen in Graphite Ablation," *AIAA Journal*, Vol. 14, No. 11, 1976, pp. 1640–1642.
doi:10.2514/3.7267
[8] Allendorf, H. D., and Rosner, D. E., "Primary Products in the Attack of Graphite by Atomic Oxygen and Diatomic Oxygen about 1100 K," *Carbon*, Vol. 7, No. 4, 1969, pp. 515–518.
doi:10.1016/0008-6223(69)90086-4
[9] Rosner, D. E., and Allendorf, H. D., "High Temperature Oxidation of Carbon by Atomic Oxygen," *Carbon*, Vol. 3, No. 2, 1965, pp. 153–156.
doi:10.1016/0008-6223(65)90042-4
[10] Blackwood, J. D., and McTaggart, F. K., "Oxidation of Carbon with Atomic Oxygen," *Journal of Chemistry*, Vol. 12, 1959, pp. 114–121.
[11] Suzuki, T., Fujita, K., and Sakai, T., "Graphite Nitridation in Lower Surface Temperature Regime," *Journal of Thermophysics and Heat Transfer*, Vol. 24, No. 1, 2010, pp. 212–215.
doi:10.2514/1.43265